A conceptual framework for shear flow–induced erosion of soft cohesive sediment beds

J. C. Winterwerp,[1,2] W. G. M. van Kesteren,[2] B. van Prooijen,[1] and W. Jacobs[1,3]

Received 20 March 2012; revised 24 August 2012; accepted 11 September 2012; published 24 October 2012.

[1] This paper proposes a conceptual framework for erosion of cohesive sediment beds. We focus on cohesive beds, distinguishing between floc erosion, surface erosion, and mass erosion. By (our) definition, surface erosion is a drained soil mechanical process, whereas mass erosion occurs under undrained conditions. The eroding shear stress is modeled through a probability density function. This yields a continuous description of floc erosion and surface erosion as a function of mean bed shear stress. Furthermore, we assume a distribution for the bed strength. The mean values of the bed strength are derived from soil mechanical theory, assuming that the surface erosion rate is limited by the swelling rate from the undrained shear strength in the bed to its drained value at its surface. The rate of erosion then relates to the undrained shear strength of the soil, and its consolidation (swelling) coefficient. The critical shear stress for erosion is slightly larger than the true cohesion of the bed, i.e., the drained strength, and follows a power law relation with the plasticity index. The conceptual framework proposed herein has been validated against a limited number of experimental data, and has a series of advantages above other methods of direct measuring erodibility, as it is inexpensive and can be used to attain space-covering information on the sediment bed. Moreover, the use of bulk soil mechanical parameters accounts implicitly for the effects of organic material, though the role of, e.g., macrophytobenthos mats and/or bioturbation is difficult to capture a priori.

Citation: Winterwerp, J. C., W. G. M. van Kesteren, B. van Prooijen, and W. Jacobs (2012), A conceptual framework for shear flow–induced erosion of soft cohesive sediment beds, *J. Geophys. Res.*, *117*, C10020, doi:10.1029/2012JC008072.

1. Introduction

[2] The transport and fate of fine, cohesive sediments often plays an important role in the management of estuarine and coastal waters, and in assessing the impact of engineering works on the environment. One of the key factors in this transport and fate is the exchange of fine sediment between the sea or river bed and the water column above. For this reason, the erosion of cohesive sediment beds has been studied extensively.

[3] *Partheniades* [1962, 1965, 1986] was the first to carry out erosion experiments on marine cohesive sediments in a systematic way; he summarized his findings recently in *Partheniades* [2010]. The first experiments were done with mud from San Francisco Bay in a straight, recirculating flume with Bay water. Later, Partheniades also used industrial clays. The first series of erosion experiments were carried out on a placed, remolded bed at in situ density, and the second series was done on so-called deposited beds, formed through deposition and subsequent consolidation from a cohesive sediment suspension. Deposited beds form from virgin consolidation and are characterized by vertical gradients in sediment properties. Partheniades' results are presented in Figure 1.

[4] Both experiments showed a small, nonzero erosion rate at the smallest bed shear stresses applied. This indicates that a threshold shear stress (critical shear stress for erosion) would not exist, or is very small. In his data analysis, Partheniades assumed a Gaussian bed shear stress distribution, and obtained the following formula for the erosion rate E [kg/m^2/s]:

$$E = \frac{AD_{50}\rho_s}{t^{(\tau_b)}}\left[1 - \frac{1}{\sqrt{2\pi}}\int_{-\frac{c}{k\eta_b\bar{\tau}_b}-\frac{1}{\eta_b}}^{\frac{c}{k\eta_b\bar{\tau}_b}+\frac{1}{\eta_b}} \exp\left\{-\frac{\omega^2}{2}\right\}\mathrm{d}\omega\right] \qquad (1)$$

in which A and k are empirical coefficients, D_{50} is the median diameter of the bed forming flocs, $t^{(\tau_b)}$ is the time that the time-varying bed shear stress exceeds the cohesive forces within the bed, c is the cohesion due to interparticle forces, $\bar{\tau}_b$ is the mean bed shear stress with $\eta_b\bar{\tau}_b$ its variance, and ω is a dummy variable.

[1]Civil Engineering and Geosciences, Environmental Fluid Mechanics, Delft University of Technology, Delft, Netherlands.
[2]Deltares–Delft Hydraulics, Delft, Netherlands.
[3]Royal Boskalis Westminster Ltd., Papendrecht, Netherlands.

Corresponding author: J. C. Winterwerp, Civil Engineering and Geosciences, Environmental Fluid Mechanics, Delft University of Technology, PO Box 5048, NL-2600 GA Delft, Netherlands. (han.winterwerp@deltares.nl)

0148-0227/12/2012JC008072

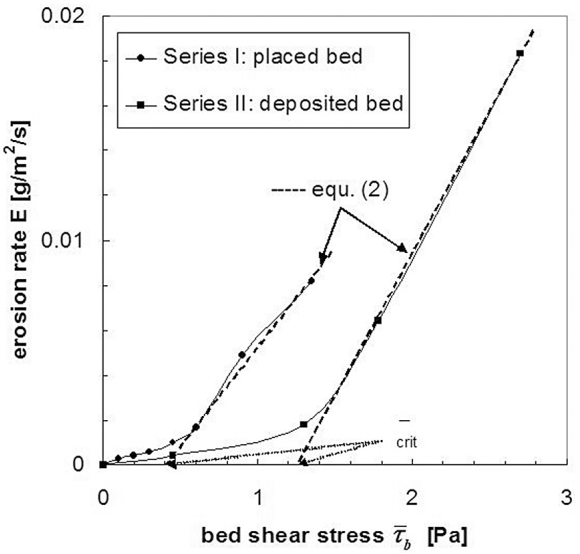

Figure 1. Erosion rates measured by Partheniades (redrawn from *Partheniades* [1965]).

[5] Similar results were found by *Christensen and Das* [1974] and *Croad* [1981], with different coefficients however.

[6] *Kandiah* [1974] and *Ariathurai and Arulanandan* [1978] parameterized Partheniades' results:

$$E = M\left(\frac{\bar{\tau}_b - \tau_{cr}}{\tau_{cr}}\right) \quad \text{for} \quad \bar{\tau}_b > \tau_{cr} \tag{2}$$

where M [kg/m^2/s] is an erosion rate parameter, $\bar{\tau}_b$ the mean bed shear stress, and τ_{cr} a critical (threshold) shear stress for erosion. This formula was combined with the so-called Krone's deposition formula describing water-bed exchange rates in numerical models for the transport of cohesive sediment. This combination is commonly known as the Krone-Partheniades bed-boundary condition. *Winterwerp* [2007] [also *Winterwerp and van Kesteren*, 2004] argued that *Krone*'s [1962, 1993] deposition formula in fact models the simultaneous erosion and deposition of fine sediments in Krone's flume experiments. However, in the present paper we deal with the erosion part of the water-bed exchange processes only.

[7] Note that the inclusion of τ_{cr} in the denominator of equation (2) is attractive from a dimensional point of view. However, applying equation (2) can introduce inaccuracies in establishing M from erosion experiments, as M then becomes sensitive to small errors in τ_{cr} near the onset of erosion. Moreover, some erosion already occurs at $\bar{\tau}_b < \tau_{cr}$, e.g., Figure 1, which is often referred to as floc erosion.

[8] Following the work by Partheniades, many more erosion experiments were carried out, in particular in the 1970s and 80s. Many were done in (rotating) annular flumes, which are circular flumes with a rotating lid to drive the flow. Often, the flume itself can rotate in opposite direction to minimize secondary currents. Such a flume was applied by *Mehta and Partheniades* [1975] on deposition experiments, and later for erosion experiments on kaolinite beds [*Mehta and Partheniades*, 1979].

[9] The common test procedure studying erosion in a (rotating) annular flume is as follows. A placed or deposited bed (see below) is prepared in the flume, and the flow velocity is increased in small steps. Each step is maintained for a fixed period, generally ten minutes to about 1 h, and the increase in suspended sediment concentration in the flume (i.e., the amount of eroded material) is measured. A typical example of the results of such experiments is given in Figure 2, showing the increase in suspended sediment concentration in an annular rotating flume as a function of the bed shear stress, as measured by *Kuijper et al.* [1990] for mud from the Western Scheldt estuary, The Netherlands.

[10] The erosion formula (2) has been generalized [*Harrison and Owen*, 1971; *Kandiah*, 1974; *Mehta*, 1981; *Lick*, 1982; *Sheng*, 1986], and used (in mathematical models) throughout the world, no doubt because of its simplicity:

$$E = M\left(\frac{\bar{\tau}_b - \tau_{cr}(z,t)}{\tau_{cr}(z,t)}\right)^n \quad \text{for} \quad \bar{\tau}_b > \tau_{cr} \tag{3}$$

where t = time and z = vertical coordinate into the bed. The exponent n is generally unity, though other values have been proposed [*Harrison and Owen*, 1971; *Kusuda et al.*, 1984]. The critical bed shear stress for erosion τ_{cr} is generally assumed to be a constant material parameter, but may vary with depth and time because of consolidation and physico-chemical effects. Typical values given in literature are: 0.1 Pa $< \tau_{cr} <$ 5 Pa. In addition, the erosion parameter M may vary with time and depth, but is commonly kept constant as well; typical values are: 0.01×10^{-3} kg/m^2/s $< M < 0.5 \times 10^{-3}$ kg/m^2/s. A summary on parameter values for mud from English estuaries is given by *Whitehouse et al.* [2000]. It should be noted that τ_{cr} and M can be (much) smaller or larger, in particular for consolidated clay deposits and/or under the influence of biota. For instance, *Le Hir et al.* [2007] found high values of τ_{cr} up to 4 Pa depending on the Chlorophyll *a* content.

[11] Equation (3) is commonly applied to well-consolidated, homogeneous beds, in which case τ_{cr} and M are more or less constant throughout the bed. This type of erosion is

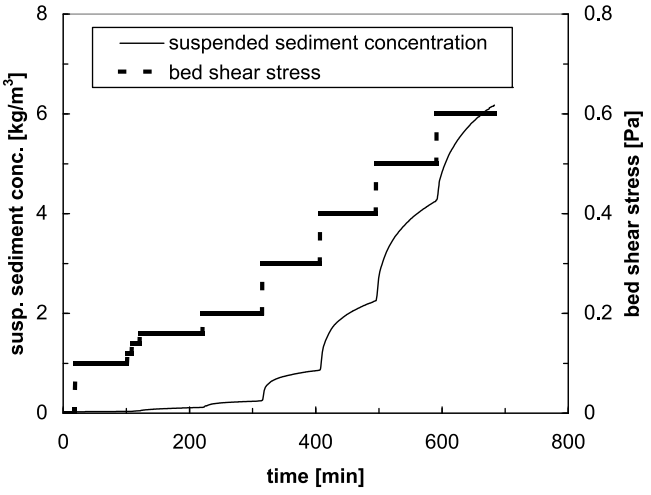

Figure 2. Typical example of applied bed shear stress and suspended sediment concentration in rotating annular flume [after *Kuijper et al.*, 1990].

sometimes referred to as unlimited (Type II) erosion in the literature, and is studied in the laboratory on so-called placed beds. Such placed beds are made from a homogenized mud slurry; the slurry is brought in the experimental facility, and its surface is leveled manually; sediment properties are more or less constant with depth.

[12] Limited erosion (Type I) is characterized by erosion rates decreasing in time (with depth) at constant forcing (as in Figure 2). This behavior has been explained from increasing bed strength with depth (the bed is stratified) or by armoring. At that depth where the bed shear stress attains the critical bed shear stress, erosion stops. This type of erosion is therefore also called depth-limited or supply limited erosion, and can be studied in the laboratory with beds obtained through sedimentation and consolidation from a relatively dilute suspension (so-called deposited beds). *Mehta and Partheniades* [1979] carried out erosion experiments on such stratified beds, and proposed the following erosion formulation:

$$E = E_f \exp\left\{\alpha\left(\frac{\bar{\tau}_b - \tau_{cr}(z)}{\tau_{cr}(z)}\right)^{\beta}\right\} \tag{4}$$

where E_f [kg/m^2/s] is referred to as the floc erosion rate, α and β are material dependent parameters and $\tau_{cr}(z)$ is a depth-varying critical shear stress for erosion. This formula was applied by, e.g., *Parchure and Mehta* [1985] and *Amos et al.* [1992]. Typical values for the various parameters are: 0.003×10^{-3} kg/m^2/s $< E_f < 5 \times 10^{-3}$ kg/m^2/s; $0.5 < \beta < 1$; $5.0 < \alpha < 15.0$ and 0.01 Pa $< \tau_{cr} <$ 0.1 Pa.

[13] *Sanford and Maa* [2001] showed that equations (4) and (2) may yield identical erosion rates under the assumptions that in equation (2) $\tau_{cr} = \tau(z)$, $d\tau_{cr}/dz$ = constant, $M = M(z) = \eta' \rho_b(z)$, with bulk density ρ_b and η = constant. They argue further that the time-scale of the eroding forces in relation to the time-scale of erosion determines whether the erosion process is unlimited or depth-limited. This observation is qualitatively similar to the analysis in this paper on the role of the permeability of the soil, as discussed below. Recently, *Sanford* [2008] added an empirical consolidation model to this equation to account for varying vertical gradients in bed strength.

[14] Though the erosion formulae given above are simple from a mathematical point of view, and easily implemented into numerical models, their coefficients can only be obtained from painstaking experiments, or from trial-and-error calibration of numerical models. Therefore, we seek an alternative formulation with coefficients that can be measured more easily. Here, we propose a conceptual framework for the erosion of cohesive sediment beds by shear flow, induced by currents, tides and/or waves (orbital movements). We limit ourselves to beds with little sand, well away from the transition between granular and cohesive behavior of sediment beds [e.g., *Van Ledden et al.*, 2004; *Jacobs*, 2011]. In this framework, we distinguish between so-called floc erosion, surface erosion and mass erosion, providing a scheme for their occurrence including a smooth transition from one mode to the other.

[15] Our framework is based on a combined hydrodynamic and soil mechanical approach. The hydrodynamic component, proposed before by *Van Prooijen and Winterwerp* [2010], addresses the eroding forces by the shear flow, in which turbulent fluctuations in the stresses are explicitly accounted for. A linear function was assumed between the relative erosion rate and the relative turbulence-mean bed shear stress. Full details are given by *Van Prooijen and Winterwerp* [2010], a summary of which is given in section 6. This section also discusses simulations of an erosion experiment by *Jacobs* [2011], applying his soil mechanical coefficients.

[16] In the soil mechanical component, we discuss in detail the role of pore water pressure gradients induced by deformations of the soil at microscale. Section 2 contains a brief description of the relevant soil mechanical principles and the definition of a number of soil mechanical parameters, used elsewhere in this paper. Our approach is limited to soils with a cohesive behavior, and we discuss in section 3 how the onset of cohesion can be determined easily from soil mechanical parameters, and how the strength of the bed can be measured with simple tools. We distinguish between surface erosion, a process not affected by water under pressures, and mass erosion, a process fully governed by water under pressures. In section 4 we discuss the onset of surface erosion, and the erosion rate, presenting simple formulae with easily measurable parameters, whereas in section 5 we discuss the process of mass erosion.

[17] We note that some material in the present paper has been published before, but not in its present context. Some redundancy is therefore unavoidable, presenting a complete and consistent picture on the erosion of cohesive sediment beds by shear flowinduced stresses.

2. Soil-Mechanical Background

[18] In this paper, the response of a bed/soil to hydrodynamic loading by shear flow is assumed to be governed by soil-mechanical failure, weakening/destroying the bonds between soil particles to such extent that these particles can be picked up by a turbulent flow. We treat the bed as a two-phase continuum, i.e., a solid phase and a fluid phase, even though we discuss some processes at the scale of individual particles and the surrounding pore water. Our focus is on cohesive beds only; in section 3 we describe the transition between the cohesive and noncohesive response of a bed. Moreover, we limit ourselves to cohesive beds in alluvial systems, i.e., our framework is applicable for weakly to fairly consolidated beds. In this paper, we exclude stiff clays, or fluffy sediment layers formed during slack water in tidal environments.

[19] In this section, we summarize the soil mechanical concepts relevant for our framework. Though these concepts have been established decades ago, and are explained in most (classical) textbooks on soil mechanics [e.g., *Lambe and Whitman*, 1979; *Whitlow*, 2001], they have not been brought together describing the erosion of soft, cohesive sediment beds. Part of this summary has been described in *Winterwerp and van Kesteren* [2004].

[20] It is most illustrative to start our reasoning at microscopic scale, i.e., at the scale of the soil particles. When these particles are eroded/displaced from the bed surface by turbulent shear flow, their place has to be filled with water, because of continuity.

[21] Turbulent stresses on a particle (lift forces) induce local (pore) water under pressures, which are a function of the rate of deformation (erosion rate) and the dissipation rate

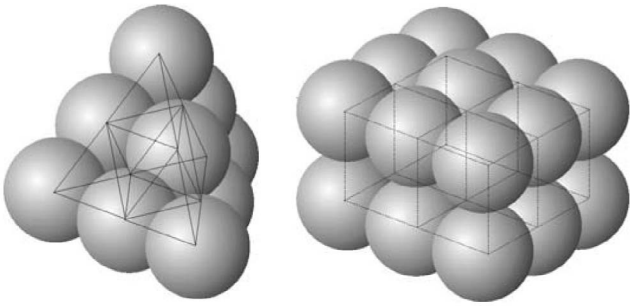

Figure 3. Schematic granular arrangement with (left) dense skeleton, and (right) loose skeleton, the critical state packing (deformations without macroscopic volume changes) is somewhere in between these two extremes.

of the induced water under pressure, the latter being a function of the permeability of the soil. The ratio between the rate of deformations and the infill rate of pore water is measured with the Péclet number. Large Péclet numbers refer to undrained conditions, commonly occurring in cohesive soils because of their low permeability. Low numbers refer to drained conditions, and pore water pressure gradients are dissipated rapidly.

[22] The water under pressures hamper the deformation of the soil, e.g., the erosion of particles from the soil: the bed strength seems to increase. This apparent strength is referred to as apparent cohesion, which, in contrast to the true cohesion of the soil, is a function of the deformation rate and permeability (hence structure) of the soil. The true cohesion is a soil property, depending mainly on electro-chemical bonds between the particles, often enhanced by organic polymers in the soil (poly saccharides, such as EPS), as explained below. It is noted that for soft cohesive sediments true cohesion typically amounts 0.1–1 Pa, whereas apparent cohesion exhibits values of 1–100 Pa.

[23] One scale larger, at the mesoscale of groups of particles, the packing of the soil becomes important. Figure 3 presents a cartoon of two possible states of a granular soil, a dense packing in the left panel and a loose configuration in the right panel. Upon loading, assuming incompressible water and unbreakable (primary) particles, deformation of densely packed soils requires the soil to dilate, expanding in total volume: water has to flow into the soil.

[24] Stresses exerted on the right panel configuration of Figure 3 generally result in contraction of the soil, and water is driven out. Under undrained conditions quick sand or quick clays may be formed. This configuration is not relevant for the erosion of natural deposits of cohesive sediment beds by shear flow.

[25] In between these two extreme granular arrangements (e.g., a dense and a loose soil) there should be a packing at which deformation of the soil takes place without volume change (no dilation, nor contraction). This state of the soil is known as the "critical state." Note that this state is characterized by some particle interlocking (e.g., Figure 3), and that, upon deformation, some particle rearrangement at microscale is required along planes of failure.

[26] In analyzing the response of a soil sample at macroscopic scale, use is made of the effective stress concept in which the total stress σ is assumed to be composed of an effective part σ' and the pore water pressure p^w:

$$\sigma = \sigma' + p^w \tag{5}$$

Note that the effective stress σ' represents the average stress carried by the soil skeleton, and therefore does not represent the (microscopic) interparticle stresses.

[27] The response at this scale can be described conveniently by analyzing the response of a soil sample subject to a triaxial test. A cylindrical sample, supported by a thin membrane, is placed in a so-called triaxial cell. Within this cell, an isotropic stress can be set, loading the sample with a so-called cell pressure $\sigma'_1 = \sigma'_2 = \sigma'_3$, where σ'_i are (effective) principal stresses. As pore water can escape under drained conditions, excess pore water stresses cannot build up, and one measures changes in effective stress only. Next, the vertical principal stress σ'_1 is increased by loading the top of the sample, as sketched in Figure 4, until failure occurs (depicted by "loading 2"). As no pore water pressure builds up under drained conditions, failure of the soil occurs through failure of the granular skeleton. This procedure is repeated a number of times (on different samples), while varying the cell pressure ("loading 1").

[28] More generally, triaxial tests can be carried out under drained and undrained conditions. Under drained conditions, σ'_1–σ'_3 combinations of stresses at failure can be plotted in a shear stress (τ) – normal stress (σ) diagram. In this so-called Mohr-diagram, σ'_1 and σ'_3 support the Mohr circles, from which also (normal and shear) stresses other than the principal stresses can be read. The envelope around these circles forms the Mohr-Coulomb failure envelope:

$$\tau = c' + \sigma' \tan\{\phi'\} \tag{6}$$

where a prime refers to effective stresses. The slope of the envelope ϕ' represents the angle of internal friction, and its crossing with the ordinate yields the true cohesion of the soil, c', i.e., the drained strength c_d at zero normal stress. Note that for cohesive soils, the Mohr-Coulomb failure envelope is curved, indicative for the power law behavior of the material (see below). Cohesive stresses typically amount to O{0.1–10} Pa for the soft soils subject of this paper, hence these are typical values for the drained shear strength. The slope at which the sample fails, θ_{cr}, can be read from the Mohr circles, as indicated in Figure 4. The cohesion c' and angle of internal friction ϕ' are true soil properties, depending on clay mineralogy, organic polymers and pore water chemistry.

[29] However, drained triaxial tests on cohesive soils are cumbersome because of their low strength (difficult to prepare a proper sample) and low permeability (tests take a long time). Therefore, undrained triaxial tests are more common, in which case part of the external load is carried by the pore water, and the effective stresses become independent of the back pressure in the triaxial cell. The shear stress (at failure) then becomes equal to half the difference between the two principal total stresses, which equals the difference between the two principal effective stresses, as pore water stresses are isotropic. At failure, this shear stress is referred to as the

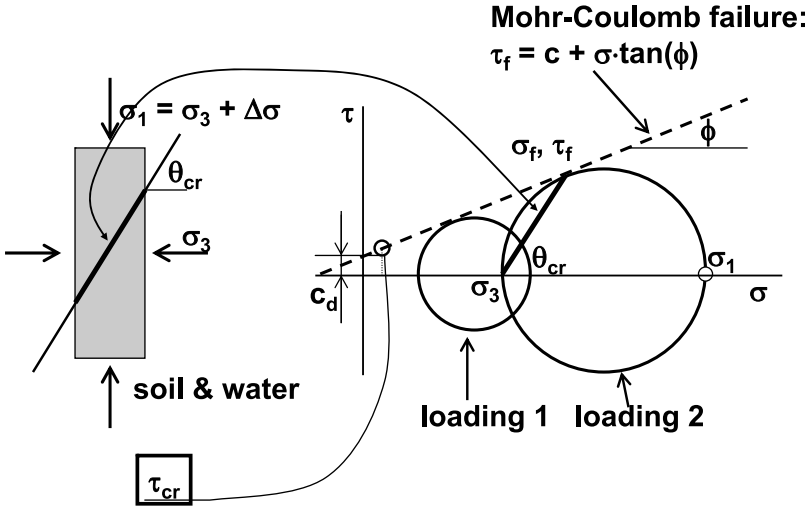

Figure 4. Sketch of a drained triaxial test—the sample fails at the effective stresses σ'_1 and σ'_3, shown in the Mohr diagram in the right. From a family of stresses at failure, the so-called Mohr-Coulomb failure envelope is constructed. The stress diagram also shows the angle of internal friction ϕ', the true cohesion c_d (=c') and the critical shear stress for erosion τ_{cr}. All primes on the stress symbols have been deleted in this figure to improve readability. Note that for cohesive sediment, the Mohr-Coulomb envelope is often convex (see below).

undrained shear strength c_u:

$$c_u = (\sigma_1 - \sigma_3)/2 = (\sigma'_1 - \sigma'_3)/2 \quad (7)$$

Hence, the drained shear strength and angle of internal friction cannot be established directly, unless pore water stresses are measured as well. Moreover, the envelope around the Mohr circles at failure for the total stress yields a line parallel to the abscissa, representing this undrained shear strength c_u at its crossing with the ordinate.

[30] Scaling down our observations, we note again that failure of a densely packed soil implies local dilatation around the plane of failure until the critical state is attained (locally). The undrained shear strength thus represents the stress at the critical state of the soil sample, and depends on the (local) structure of the granular skeleton. However, c_u is not a soil property, being dependent on the structure (packing) of the soil. Therefore, c_u should be considered as a property of the soil sample and its state (e.g., its physico-chemical properties and its structure/density). Hence, c_u is expected to increase with depth into the bed because consolidation enhances bulk density.

[31] Unfortunately, undrained triaxial tests on soft soils are not easily performed either, as the samples are difficult to support within the cell's membrane. Therefore, we advocate shear vane tests to determine the undrained shear strength. That test should be carried out fast enough to guarantee undrained conditions. From the reasoning above on the soil response at microscale, we expect a (small) overshoot in stresses prior to failure of the soil owing to local dilation toward the critical state. The shoulder in stress directly after this peak represents the undrained shear strength c_u (see section 3).

[32] At this third macroscopic spatial scale, the consistency of a soil can also be described by its degree of "fluidness" or "solidness." Cohesive materials exhibit a gradual transition from fluid-like behavior to solid-like behavior—this transitional zone is referred to as plasticity. Heuristic tests were developed defining the transition of soil behavior from fluidness to plastic, and from plastic to solid. These two transitions concern water contents referred to as the liquid limit (LL) and the plastic limit (PL). From an almost infinite data set, it is found that the undrained shear strength of a soil c_u at the liquid limit amounts to about 1–2 kPa, and at the plastic limit to about 100–200 kPa. Note that in reality, soil properties vary gradually around the LL and PL.

[33] The liquid and plastic limit belong to the family of the so-called Atterberg limits, which define the water content W (weight of pore water divided by the dry weight of solids) of the soil at these limits. Note that traditionally in soil mechanics, the Atterberg limits are given in percentage, and we follow that tradition. The difference between the liquid and plastic limit is referred to as the plasticity index PI = LL − PL. Montmorillonite clays have large PI, whereas sands have PI = 0. Cohesive behavior is found to be encountered around PI > 7% [e.g., *Lambe and Whitman*, 1979; *Whitlow*, 2001]. Though highly empirical, the Atterberg limits provide much information on the behavior of a soil. For instance, when the water content (soil's bulk density) is normalized with the plasticity index through the liquidity index LI (LI = (W − PL)/PI), the undrained shear strength and soil permeability can be related to the Atterberg limits [e.g., *Winterwerp and van Kesteren*, 2004].

[34] The Atterberg limits are determined by drying a soil sample or adding water (preferably with local water, i.e., with proper pH and salinity) to the sample until the plastic and liquid limits are found. This implies that the effects of organic polymers, salinity, etc. are largely maintained provided the samples are not too much heated while drying.

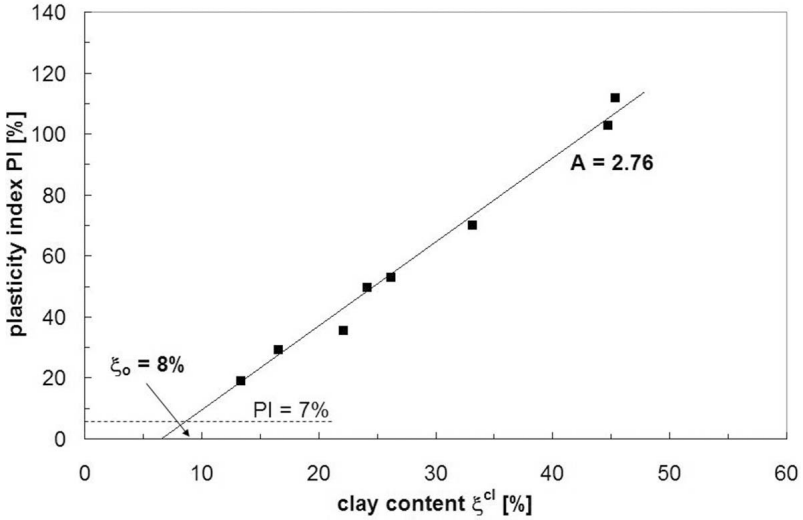

Figure 5. Activity-plot for IJmuiden mud [*Winterwerp and Van Kesteren*, 2004]; onset of cohesive behavior for this soil is predicted at ξ_o = 8% clay content at PI = 7%.

However, the mechanical effects of biota (bioturbation and/or bio-stabilization) are lost. Note that these measurements have been standardized throughout the world, but require quite some experience to obtain accurate and reproducible results.

[35] The mechanical behavior of soils at macroscale is governed largely by drainage, as the undrained shear strength is very much larger than the drained strength, provided the soil's packing is not too loose. This influence of drainage is therefore also observed in the response of the bed to shear flow–induced stresses. When these stresses exceed a certain threshold, erosion of the bed occurs. In case of drained conditions, we refer to surface erosion in this paper. Under undrained conditions, we refer to mass erosion.

[36] The primary assumption in this paper is that the drained process of surface erosion occurs at the critical state of the sediment. When the sediment is over-consolidated (for instance when layers of sediment have been removed from the bed, or when the turbulent stresses exceed some threshold value), the bed needs to swell to attain drained conditions. Upon such swelling (e.g., following the so-called swelling line), the effective stress within the bed scales as $e \propto \sigma'^{-C_S}$, in which e is the void ratio and C_s is known as the swell index [*Lambe and Whitman*, 1979; *Mitchell*, 1976].

[37] In case of normal consolidation, a so-called virgin bed is formed, in which the effective stress scales as $e \propto \sigma'^{-C_c}$, in which C_c is known as the compression index. During normal consolidation, the stresses follow the so-called compression line. For clayey sediments, the ratio between C_c and C_S varies between about 3 and 7, with the larger values for montmorillonite clays [e.g., *Lambe and Whitman*, 1979; *Mitchell*, 1976]. When the sand content increases, this range changes further; the effects of sand however are beyond the scope of the present paper.

3. Cohesion and Strength

[38] Sedimentary beds in rivers, estuaries and coastal seas are often of mixed nature with respect to their sediment composition. In this paper, we deal with cohesive beds with little sand only. In case the bed depicts a granular response, i.e., when dominated by sand, we refer to the work by *Van Ledden* [2003], *Van Kessel et al.* [2011], and *Jacobs* [2011].

[39] *Van Ledden et al.* [2004, see also *Winterwerp and van Kesteren*, 2004] proposed a phase diagram for assessing bed response. This diagram is based on a quantification of the heuristic sedimentary triangles used in sedimentology, and the observation that the silt-clay ratio in natural systems is often more or less constant [*Flemming*, 2000]. In that case, the sediment composition of the bed can conveniently be defined with the sand content only. Here we will only summarize the onset of cohesive behavior. This onset is easily determined from an activity plot, in which the plasticity index PI is plotted as a function of the clay content ξ^{cl}; variations in clay content follow from variations in sand content. The slope of this function yields the so-called activity A, which is determined by the clay minerals at hand, and the effects of organic material (polymers). *Lambe and Whitman* [1979] give some values for mixtures of pure clay and fresh water: kaolinite: A = 0.38; illite: A = 0.9; and sodium montmorillonite: A = 7.2. For soils with not too large organic content (<15%), the clay content ξ^{cl} at PI = 7% defines the onset of cohesive behavior, reflected with ξ_0. An example of an activity plot is presented in Figure 5; the various data points reflect variations in sediment composition (sand-mud ratio).

[40] Section 4.1 presents a method determining the onset of erosion as a function of the plasticity index PI. An activity plot then allows determining the onset of cohesion. Note that theoretically, the onset of cohesion can also be determined with the triaxial tests described in section 2, but this is a highly unpractical method.

[41] Often, the strength of (soft) cohesive soil samples is determined with a roto-viscometer, which rotational speed is increased in time. This yields a so-called flow curve, a typical example of which is presented in Figure 6, showing a shear thinning behavior, characteristic for cohesive sediment beds. At the onset of deformation (very small $\dot{\gamma}$), the shear stress is poorly defined, and often a function of the experimental procedure – this shear stress is referred to as the yield strength τ_y of the sediment. A more unambiguous measure

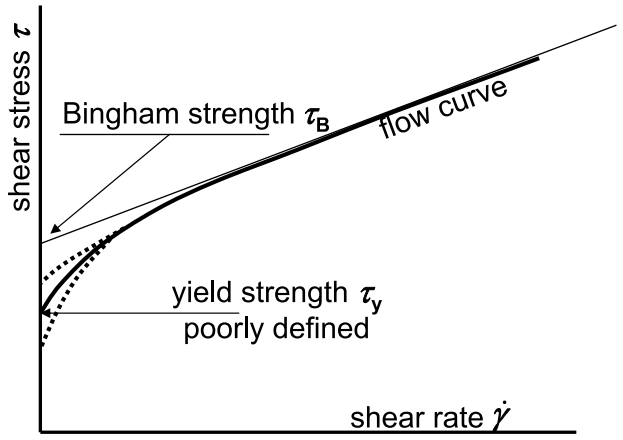

Figure 6. Sketch of a flow curve obtained with a rheometer, and definition of Bingham and yield strength τ_B and τ_y; τ_B follows from the crossing of the tangent to the flow curve with the ordinate.

is the Bingham strength τ_B, obtained from the crossing of the tangent to the flow curve with the ordinate.

[42] As it is difficult to prevent drainage in a roto-viscometer experiment, τ_y is often affected by drainage, and reflects a lower value of the actual undrained shear strength c_u of the material. At larger shear rates, deformation rates are large, and more undrained conditions prevail – the Bingham strength most likely will overestimate the undrained shear strength c_u. Therefore, we expect $\tau_y < c_u < \tau_B$.

[43] Figure 7 presents data on τ_y and τ_B measured on various sediment samples from open waters in The Netherlands to get a feeling on the type of sediments with their strengths addressed in this paper. Open symbols represent samples with fairly low clay contents and relative high sand content (but still more or less cohesive). The gray-colored area in Figure 7 depicts characteristic values for c_u for these samples. In the following sections we deal with relatively freshly deposited sediment beds, with bulk densities below around 1300–1400 kg/m^3, hence we expect values for c_u well below 0.1 kPa (see also Figure 8).

[44] In section 2, we promoted the use of simple shear vane measurements to measure the remolded shear strength, which equals the undrained shear strength c_u. However, if the samples are too soft, vane measurements may be cumbersome, and roto-viscometer measurements may be inevitable. Then, we have to rely on our observation that c_u should lie in between the yield strength τ_y and the Bingham strength τ_B measured with such a roto-viscometer.

4. Surface Erosion From a Soil Mechanical Perspective

4.1. Onset of Erosion

[45] It is obvious that particles can be removed from the bed only when the flow-induced stresses exceed the strength of the bonds, which keep the particles in/on the bed. This strength is referred to as the critical shear stress for erosion, and it relates to the true cohesion, or drained strength of the sediment at the bed surface (e.g., section 2). At the sediment bed surface, the self-weight of the flocs induces some normal stresses, possibly in conjunction with some over consolidation. The effective stress at the sediment surface is therefore slightly larger than zero; we expect that τ_{cr} may be about 10% larger than the drained shear stress c_d, but ignore this subtlety in the remainder.

[46] The drained shear strength (at the sediment's surface) is a function of sediment properties (clay mineralogy, organic polymers and pore water chemistry), sediment composition (clay/sand content) and sediment structure. The sediment structure at the sediment's surface tends to its critical state by swell (e.g., section 4.2). Both strength, and swell and

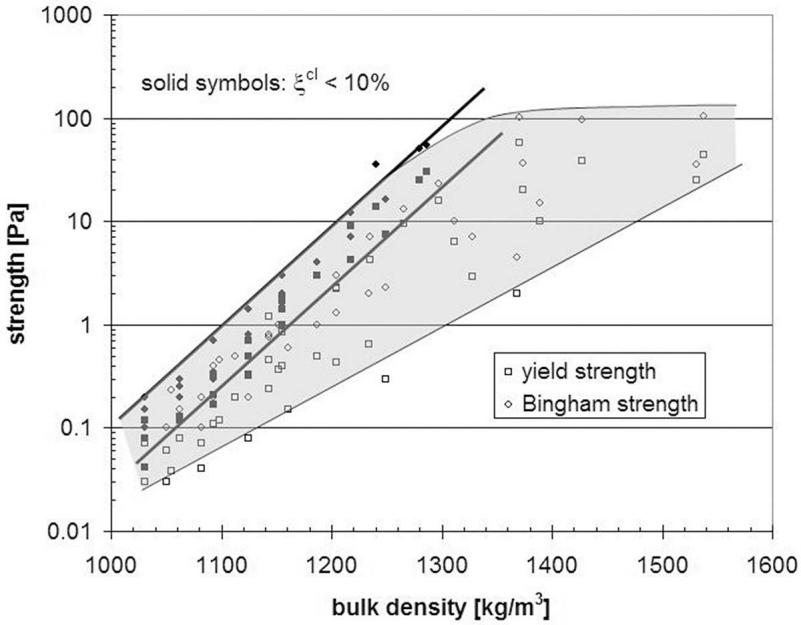

Figure 7. Measured values of yield and Bingham strength for a variety of mud samples from the Netherlands. The undrained shear strength takes values in between these strengths.

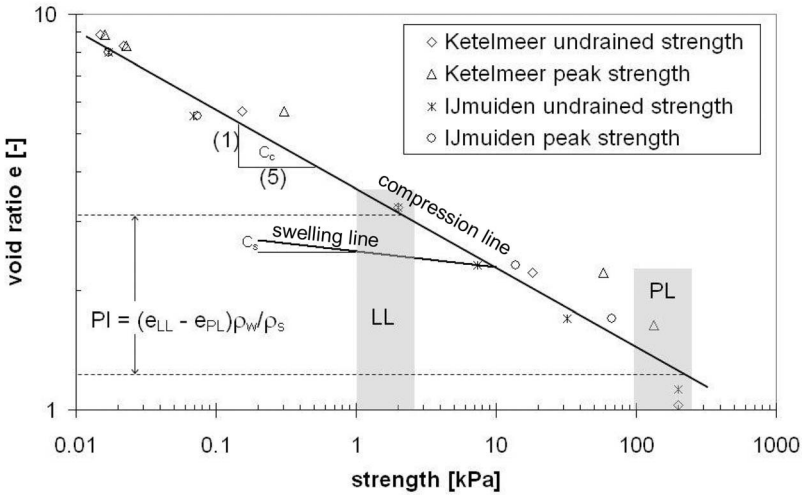

Figure 8. Vane strength measurements on mud from Lake Ketelmeer and IJmuiden Harbor. Both undrained shear strength c_u and peak strength are shown—the latter is the larger of the two. Strengths ranges at the liquid limit and plastic limit are indicated in gray, together with the plasticity index PI. Moreover, the compression and swelling lines are indicated.

consolidation can be conveniently described by fractal theory [e.g., *Kranenburg*, 1994; *Merckelbach and Kranenburg*, 2004; *Winterwerp and van Kesteren*, 2004], and can be related to the plasticity index [*Mitchell*, 1976; *Winterwerp and van Kesteren*, 2004]. As the plasticity index also reflects sediment properties (clay mineralogy and organic polymers) and sediment composition (sand content), we expect that the drained shear strength, hence the critical shear stress for erosion, is a power law function of the plasticity index.

[47] Soil mechanical theory [*Lambe and Whitman*, 1979; *Whitlow*, 2001] suggests that in theory the drained shear strength at the bed surface can be obtained from an extrapolation of strengths measured as function of the void ratio e; the latter is defined as the ratio of the fraction of voids and the fraction of solids in a soil sample. This is illustrated in Figure 8, presenting the results of vane strength measurements on normally consolidated cohesive sediments from Lake Ketelmeer and IJmuiden Harbor, The Netherlands. The peak strength values are a bit higher than the undrained shear strength c_u, as expected. All data follow a power law relation between void ratio as function of c_u with a slope of ~ -0.2. Hence, in terms of normal consolidation, where the ratio of undrained shear strength and effective stress is constant, Figure 8 suggests that for Ketelmeer and IJmuiden mud the compression index $C_c = 0.2$.

[48] If we presume that the cohesive bed is built of flocs with a self-similarity structure, the yield strength τ_y of the bed should scale with the volumetric solid concentration ϕ_s as $\tau_y \propto \phi_s^{2/(3-n_f)}$, in which n_f is the so-called fractal dimension [*Kranenburg*, 1994]. Replotting the strength data against the volumetric mass concentration ϕ_s (results not shown) yields a fractal dimension of about $n_f \approx 2.7$, well in line with numbers presented in the literature [e.g., *Kranenburg*, 1994; *Winterwerp and van Kesteren*, 2004]. It is well-known that the strength-density relation is highly nonlinear, which also follows from our fractal approach: variations in fractal dimension n_f between 2.6 and 2.8 would yield a variation in the ϕ_s-exponent between 5 and 10.

[49] However, to extrapolate Figure 8 to the critical state at the sediment's surface, e.g., to find c_d, we need to account for swelling. As indicated in section 2 the swelling occurs by reducing effective stress, resulting in increasing void ratio following a power law with a swell index C_s. The swell index is always smaller than the compression index. The void ratio e on the vertical axis of Figure 8 can be related directly to PI, and follows the compression line, as explained in section 2. For the swelling line, the void ratio increase is much smaller compared to the compression line, and therefore the plasticity index must be scaled with the ratio of swell index and compression index $\mathrm{PI}^{-C_s/-C_c}$. The critical shear stress for erosion τ_{cr} therefore scales as $\tau_{cr} \propto \mathrm{PI}^{-C_s/-C_c}$, i.e. $\tau_{cr} \propto \mathrm{PI}^{\beta}$ with $\beta = 1/7 - 1/3$. However, for fairly stiff clays, *Smerdon and Beasley* [1959] found a bit larger values for β:

$$\tau_{cr} = \gamma_{cr}\,\mathrm{PI}^{\beta} \text{ with } \gamma_{cr} = 0.163, \beta = 0.84, \text{and PI in \%} \qquad (8)$$

The critical shear stress for erosion τ_{cr} in equation (8) is to be interpreted as the mean value $\mu_{\tau,cr}$, introduced in equation (16) (see below). The self-similar approach described above implies that the Mohr-Coulomb failure envelope in Figure 4 does not follow a straight line, but should be convex, as discussed in section 2.

[50] *Jacobs et al.* [2011] carried out erosion experiments in the ERODIMETRE, an erosion device developed at Ifremer [*Le Hir et al.*, 2006]. The measured values of the onset of erosion are presented in Figure 9 together with the data by Smerdon and Beasley, experiments carried out at Deltares (Lake Ketelmeer, Kembs Reservoir and IJmuiden Harbor [e.g., *Winterwerp and van Kesteren*, 2004]), and data by *Torfs* [1995] with kaolinite, montmorillonite and natural mud). For the latter, some assumptions were made on the activity of the minerals applied in the experiments, details are found in *Jacobs et al.* [2011]. To account for low-plastic

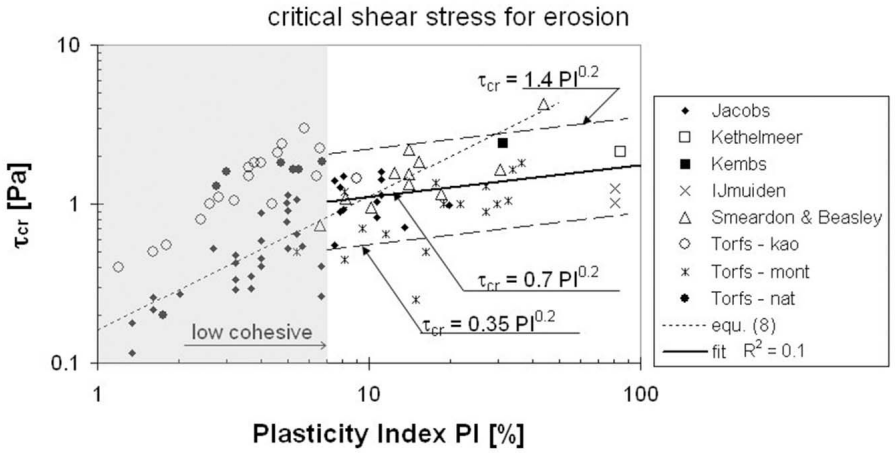

Figure 9. Critical shear stress for erosion as a function of the generalized Plasticity Index (PI); experimental data and relation (9). For PI < 7%, samples are low to non-cohesive. Power law fit only through data with PI > 7%.

sediments, *Jacobs et al.* [2011] determined PI indirectly: $PI = A(\xi^{cl} - \xi_0)$, e.g., Figure 5, referred to as the generalized plasticity index.

[51] Figure 9 shows that all data follow more or less a power law, as suggested above. While individual data sets appear to follow somewhat different power laws, as expected, it is remarkable that equation (8) as presented by *Smerdon and Beasley* [1959] characterizes most of the data reasonably well, especially at lower values of PI. The lower values are related to inactive silt and sand, which normally has a low compression index resulting in a higher ratio of swell index and compression index.

[52] Focusing on cohesive beds only, samples with PI < ~7% should be discarded in our analysis, as these are low to noncohesive—this range is indicated with the gray area in Figure 9. A fit through all data with PI > 7% yields:

$$\tau_{cr} = \gamma_{cr}\ \mathrm{PI}^{\beta} \quad \text{with} \quad \beta = 0.2 \ \text{and}$$
$$\gamma_{cr} = 0.7\ \mathrm{Pa}\ \ (0.35 < \gamma_{cr} < 1.4\ \mathrm{Pa})\ \text{and PI in \%} \qquad (9)$$

This β value lies well in between the range given above (1/7 − 1/3), though the fit for the montmorillonite data is a bit steeper, as expected, e.g., section 2.

[53] Finally, note that the Atterberg limits implicitly include the effects of sediment composition (sand-mud ratio) and of organic material (e.g., EPS, TEP, provided these polymers were not burnt by heating the soil samples). In other words, the effects of sediment composition and organic material are implicitly accounted for in equation (9).

4.2. Surface Erosion Rates

[54] When erosion is dominated by drainage (swell), as with surface erosion, the maximum erosion rate of the bed is governed by the entrainment of water into the bed. Swelling of the bed is induced in response to removal of sediment particles from the bed during erosion, and/or by the fluctuating turbulent stresses on the bed (generating pore water pressure fluctuations, hence pore water flows, e.g., *Jacobs* [2011]). The rate of swelling V_s is given by *Terzaghi*'s [1943] consolidation formula, which follows from the diffusion part of the consolidation equation, where c_v is the consolidation coefficient, and δ_s a measure of the position of the swelling "front," e.g., Figure 10:

$$V_s = \frac{\mathrm{d}\delta_s}{\mathrm{d}t} = \frac{\pi c_v}{2\delta_s} \qquad (10)$$

The maximum erosion rate V_e is governed by the swelling rate ($V_e = V_s$), as the undrained shear strength of the sediment beds under consideration is generally much larger than the shear stresses induced by turbulent flow (or waves). This paper is concerned with fairly recent deposits with strength well below

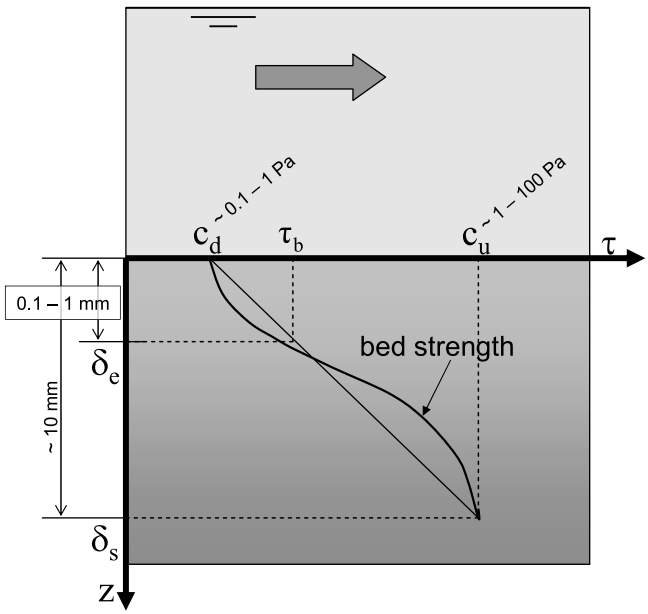

Figure 10. Sketch of swelling of the bed and strength distribution within the bed, and location of swelling front, where the bed strength amounts to c_u in response to shear flow. Characteristic values for the various parameters for soft cohesive beds are indicated. The diagram is not to scale.

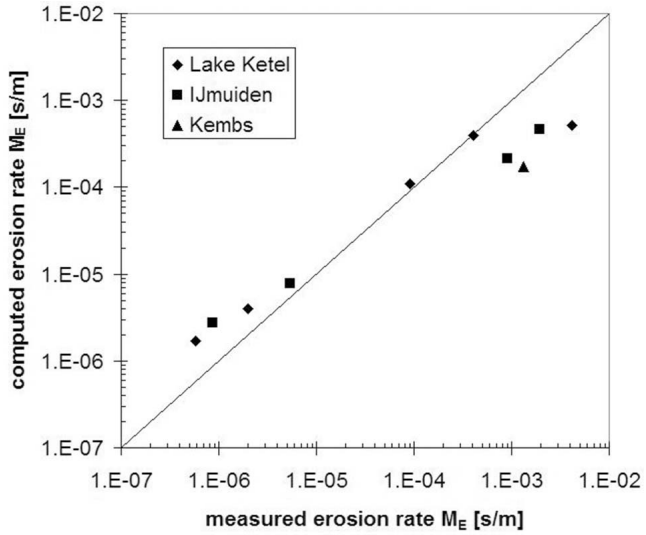

Figure 11. Comparison of erosion model (13) with various data obtained in an erosion flume in the laboratory for $\alpha = 10$ (data from non-published reports Delft Hydraulics [e.g., *Winterwerp and van Kesteren*, 2004]).

the liquid limit (e.g., Figure 7). The relation between the erodible depth δ_e and swelling depth δ_s follows from a simple linear approximation of the strength distribution within the bed, as sketched in Figure 10:

$$\delta_e \approx \frac{\tau_b - c_d}{c_u - c_d}\delta_s \approx \frac{\tau_b - c_d}{c_u}\delta_s = \frac{\tau_b - c_d}{c_u}\frac{\pi c_v}{2V_e} \approx \frac{\tau_b - \tau_{cr}}{c_u}\frac{\pi c_v}{2V_e} \quad (11)$$

where τ_{cr}, c_d and c_u have been defined before, and τ_b is the actual, instantaneous bed shear stress discussed in section 6.

[55] Finally, we need to define the thickness of the eroding layer. We anticipate that because of its drained nature, surface erosion mobilizes subsequent layers of flocs. For the time being, we assume that δ_e scales with the median diameter of the primary particles in the bed (see also section 6), corrected for interstitial water:

$$\delta_e \approx \alpha_\delta D_{50}/\phi_{s,0} \quad (12)$$

The (surface) erosion rate E [kg/m^2/s] then follows from the erosion velocity V_e [m/s] by multiplication with the dry density ρ_{dry}, which may also vary within the sediment bed:

$$E = V_E\rho_{dry} = \frac{c_v\phi_s\rho_{dry}}{\alpha D_{50}}\frac{\tau_b - \tau_{cr}}{c_u} = M_E(\tau_b - \tau_{cr});$$
$$M_E = \frac{c_v\rho_{dry}}{\delta_e c_u} = \frac{c_v\phi_s\rho_{dry}}{\alpha D_{50}c_u} \quad (13)$$

in which we defined $\alpha \equiv \pi\alpha_\delta/2$. Here we have substituted ϕ_s for $\phi_{s,0}$, as the effects of changes in water content are small in comparison to the other inaccuracies in the erosion parameters: hence, both ϕ_s and ρ_{dry} refer to the initial conditions of the soil, i.e., prior to erosion. The erosion parameter M_E [s/m] is the same as in equation (15), e.g., section 6, but different from the M parameter in section 2.

[56] The erosion formula (13) predicts that the erosion rate decreases with increasing erodible depth δ_e (e.g., floc size D_{50}), which may seem paradoxal at first glance. However, the role of δ_e cannot be analyzed in isolation, as δ_e is related to the other sediment parameters δ_s, c_d and c_u (e.g., equation (11)). In fact, equations (11), (12), and (13) imply that the swelling rate decreases with increasing floc size. In other words, the erodible depth increases with floc size, but the rate at which this erodible layer erodes, decreases with floc size. Thus, the erodible depth is not the thickness of the layer of sediment removed from the bed. Note that the inverse proportionality of the erosion rate to the median particle diameter is in agreement with common formulae on the erosion/pick-up of sand particles from the bed by turbulent shear flow [*Fernandez Luque and Van Beek*, 1976; *van Rijn*, 1984].

[57] Of course, the various parameters may vary over depth, depending on the degree of consolidation of the soil, and the effects of bioturbation. Moreover, one would expect horizontal heterogeneities as well, possibly even more important than over the vertical. Therefore, we will work with average values over the upper cm's of the bed, omitting subtleties in the spatial distribution of the bed's soil mechanical properties.

[58] Figure 11 shows the results of a series of erosion experiments on samples from Lake Ketelmeer, IJmuiden Harbor and Kembs Reservoir. These experiments were performed in a straight erosion flume, consisting of a closed conduct with rectangular diameter 0.2 m. Sediment samples were placed in a 1×0.2 m^2 container, which was suspended in the conduct with steel strings connected to force sensors, such that horizontal (bed shear stress) and vertical (changes in weight of the container, hence erosion) could be measured accurately, while the sediment's bed surface remained flush with the conduct's wall.

[59] The relevant sediment parameters are given in Table 1; these data stem from a series of laboratory experiments carried out at Delft Hydraulics. The water content at the start of the erosion experiments is depicted by W_0, and the liquidity index LI also contains information on the plasticity index PI. Figure 11 also presents the erosion parameter predicted with equation (13), using the sediment properties of Table 1 and $\alpha = 10$ (upon trial and error), showing favorable comparison with the observations, though at small erosion rates, equation (13) seems to overpredict the observations a bit, and at high erosion rates, the observations are underpredicted.

5. Mass Erosion From a Soil Mechanical Perspective

[60] When flow-induced stresses become large, stresses in the bed may exceed the local undrained shear strength, and lumps of material are torn out from the bed. This mode of erosion is referred to as mass erosion. Mass erosion is often observed for more consolidated mud deposits, as encountered on intertidal areas, c.q. mud flats, etc. The bed attains large strengths owing to physical (consolidation, drying) and biological processes (vegetation, roots, cohesion by polysaccharides, e.g., organic polymers), and sometimes chemical processes (cementing). However, also on softer beds, with strengths well below the liquid limit, mass erosion may occur,

Table 1. Parameters Erosion Experiments in Erosion Flume

	D_{50} (μm)	W_0	LI	ϕ_s	ρ_{dry} (kg/m^3)	c_v (m^2/s)	c_u (kPa)	τ_{cr} (Pa)	M_E (s/m) Computed	M_E (s/m) Measured
Ketelmeer	7.3	0.84	0.54	0.31	821	2.1×10^{-8}	18.2	n.a.	4.0×10^{-6}	1.2×10^{-6}
Ketelmeer	7.3	0.62	0.28	0.38	1005	2.1×10^{-8}	65	n.a.	1.7×10^{-6}	5.8×10^{-7}
Ketelmeer	7.3	2.15	2.10	0.15	396	2.1×10^{-8}	0.154	2.1	1.1×10^{-4}	9.2×10^{-5}
Ketelmeer	7.3	3.35	3.53	0.10	268	2.1×10^{-8}	0.015	0.2	5.2×10^{-4}	4.2×10^{-3}
Ketelmeer	7.3	3.14	3.28	0.11	284	2.1×10^{-8}	0.022	0.7	4.0×10^{-4}	4.1×10^{-4}
IJmuiden	2.5	0.87	0.56	0.30	799	6.0×10^{-9}	7.4	n.a.	7.8×10^{-6}	5.3×10^{-6}
IJmuiden	2.5	0.64	0.27	0.37	981	6.0×10^{-9}	31.9	n.a.	2.7×10^{-6}	8.7×10^{-7}
IJmuiden	2.5	2.093	2.08	0.15	405	6.0×10^{-9}	0.069	1.3	2.2×10^{-4}	9.2×10^{-4}
IJmuiden	2.5	3.03	3.24	0.11	294	6.0×10^{-9}	0.017	1.0	4.6×10^{-4}	1.9×10^{-3}
Kembs	21	0.837	1.58	0.31	823	1.8×10^{-8}	0.126	2.4	1.7×10^{-4}	1.3×10^{-3}

rupturing lumps of material from the bed [e.g., *Winterwerp and van Kesteren*, 2004].

[61] In this paper, we refer to mass erosion as an undrained erosion/scour process through which larger lumps of sediment are torn from the bed. This occurs when the stresses within the bed exceed the local strength. From our analyses above it is to be concluded that the local strength should be related to the undrained shear strength of the bed.

[62] The process of scour receives ongoing attention in the literature, no doubt because of its importance in engineering and design studies, e.g., *Hoffmans and Verheij* [1997]. Here we follow a different procedure, realizing that stresses within the bed mainly relate to the normal stresses induced by hydrodynamic loading, i.e., not to the bed shear stresses [*Sumer and Fredsøe*, 2002]. These stresses scale with the dynamic pressure $\sigma_{dyn} (\equiv {}^1/_2 \rho U^2)$, where ρ = specific density of eroding fluid (water), and U is a characteristic value of the local flow velocity (mean water velocity). Indeed, *Mazurek et al.* [2003] carried out dimensional analyses and laboratory experiments, showing that the onset of scouring and scour rates scale with $\sigma_{dyn} = {}^1/_2 \rho U_c^2$, where U_c = critical velocity for the onset of scour. Note that *Mazurek et al.* [2003] relate U_c to the critical shear stress for erosion; however our analysis above suggests a relation to the undrained shear strength.

[63] The stresses within the bed induced by (hydrodynamic) loading follow a pattern known as Prandtl's shear zones. Such shear zones are also induced by turbulent jets, and we assume that turbulent stresses within a turbulent boundary layer (shear flow) induce similar stresses. *Hill* [1985] then suggests a stability criterion:

$$\sigma_{dyn} \equiv {}^1/_2 \rho U^2 > n_{me} c_u \; ; \quad \text{with} \quad 2 < n_{me} < 5 \tag{14}$$

in which the coefficient n_{me} depends on the angle of incidence of the jet. Figure 12 presents observations on the onset of mass erosion, observed during the experiments in the straight erosion flume described above. The linear fit through the data reads $\sigma_{dyn} \sim 3.6\, c_u$, which is consistent with equation (14), though we have a few data points only.

[64] The rate of mass erosion is difficult to predict, possibly even unpredictable, as the structure of the bed, its stress history, degree of consolidation, and the effects of biota (cracks and burrowing) all play a role.

[65] We finally note that at strengths below a few Pa, the bed is so soft, that it behaves as a viscous fluid, more than a

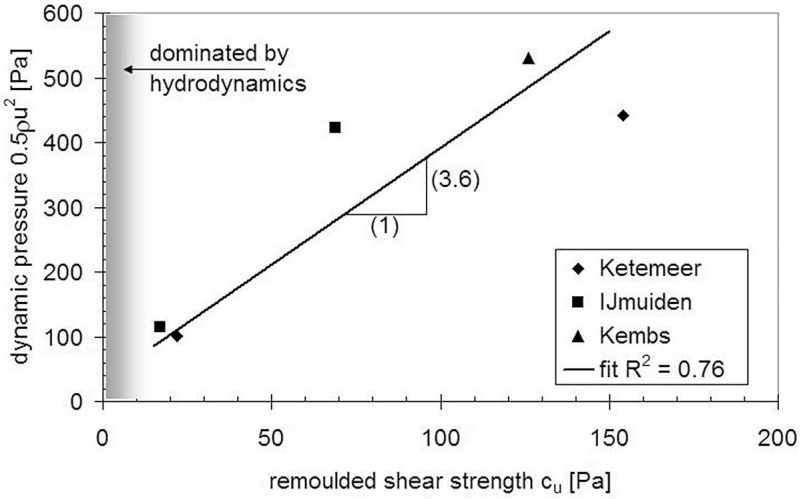

Figure 12. Onset of mass erosion from erosion experiments on mud samples from Lake Ketelmeer, IJmuiden Harbor and Kembs Reservoir; n_{me} = 3.6, e.g., equation (14).

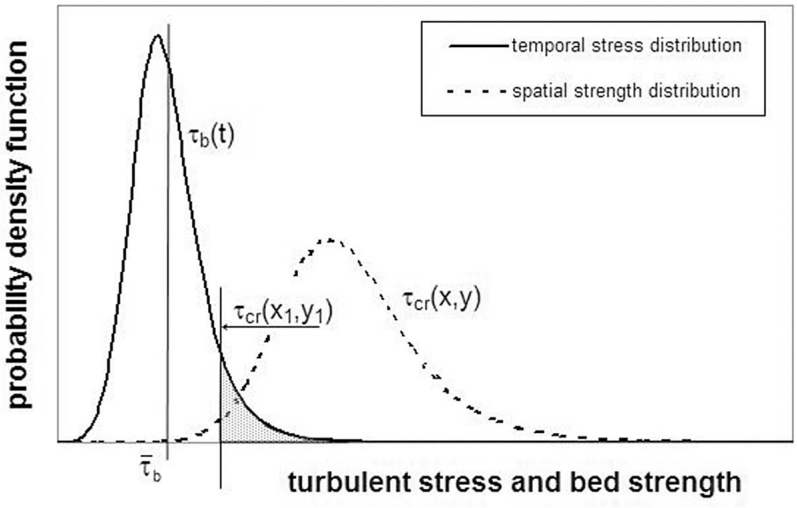

Figure 13. Sketch of spatial distribution in critical shear stress and temporal distribution in bed shear stress at the location x_1,y_1. The shaded area depicts the distribution of erosion events, tearing flocs from the bed, i.e., the conditions for floc erosion.

solid bed. Then erosion takes place in the form of entrainment by the turbulent water flow, and soil mechanical processes no longer play a role. This is depicted by a grayish band in Figure 12. The reader is referred to *Kranenburg and Winterwerp* [1997] and *Winterwerp and van Kesteren* [2004] for more details on entrainment.

6. Application

[66] The erosion rate formulation derived in section 5 is almost identical to the Partheniades' equation, e.g., equation (2). However, the sediment parameters are derived from fundamentals of soil mechanics. In this section we discuss how this approach can be used, applying the model proposed by *Van Prooijen and Winterwerp* [2010], accounting for a stochastic description of the bed shear stress.

6.1. Summary of Previous Work—Hydrodynamic Forcing by Shear Flow

[67] In this section, we briefly summarize the stochastic erosion model developed by *Van Prooijen and Winterwerp* [2010]. Let us analyze the stresses by a turbulent flow on a sediment bed at location (x_1, y_1). Generally, the strength of a bed varies spatially. For the time being, we ignore possible variations over depth, z, and only account for variations in horizontal direction x, y. This horizontal strength variation is depicted by a (Gaussian) probability density function, e.g., Figure 13. We represent the bed strength through the critical bed strength for erosion τ_{cr}, as discussed in section 4.1, which varies over space as well. At the location x_1, y_1, the relevant strength of the bed amounts to $\tau_{cr}(x_1, y_1)$. We anticipate that if the τ_{cr}-distribution is very wide (variance in τ_{cr} is large), erosion rates in the real world will be difficult to predict, as it will be difficult to collect representative samples.

[68] The instantaneous bed shear stress, induced by turbulent flow, varies over space and time. In Figure 13 we also sketch the probability density distribution of the bed shear stress at location x_1, y_1 $\tau_b(x_1,y_1,t)$. In this particular case, the mean (time-averaged) bed shear stress $\bar{\tau}_b$ is smaller than the critical bed strength for erosion τ_{cr} at that location. However, during part of the time, $\tau_b > \tau_{cr}(x_1, y_1)$, and flocs are disrupted from the bed surface, as shown in Figure 13. We refer to this condition as floc erosion.

[69] At increasing flow velocities (bed shear stresses), surface erosion may occur. In this case, sediment is torn off from the bed at a rate such that the state of consolidation of the bed can respond to changes in stress levels – of course, floc erosion continues.

[70] *Van Prooijen and Winterwerp* [2010] proposed a model for the bed shear stress distribution, and presented a parameterized form of that distribution to circumvent iteration of the implicit formula in numerical models. This parameterization yields the following erosion formula:

$$\frac{E}{M_E\tau_{cr}} = \begin{cases} 0 & \text{for } \dfrac{\bar{\tau}_b}{\tau_{cr}} < 0.52 \\ \alpha_1\left(\dfrac{\bar{\tau}_b}{\tau_{cr}}\right)^3 + \alpha_2\left(\dfrac{\bar{\tau}_b}{\tau_{cr}}\right)^2 + \alpha_3\left(\dfrac{\bar{\tau}_b}{\tau_{cr}}\right) + \alpha_4 & \\ \dfrac{\bar{\tau}_b}{\tau_{cr}} - 1 & \text{for } \dfrac{\bar{\tau}_b}{\tau_{cr}} > 1.7 \end{cases} \quad (15)$$

in which an overbar reflects turbulence-mean quantities, and for which the following parameters have been found: $\alpha_1 = -0.144$; $\alpha_2 = 0.904$; $\alpha_3 = -0.823$; $\alpha_4 = 0.204$ [e.g., *Van Prooijen and Winterwerp*, 2010]. This formulation yields a smooth transition from no erosion for $\bar{\tau} < 0.52\tau_c$ to the linear erosion formulation (equation (13)) for high bed shear stresses ($\bar{\tau} > 1.7\tau_c$). Equation (15) can be regarded as a smoother form of the Partheniades' equation, but without τ_{cr} in the denominator.

[71] *Van Prooijen and Winterwerp* [2010] completed the stochastic erosion model with a layered bed description, consisting of a thin active layer (with thickness Δ, amounting to several tens μm's) on top of a substrate (buffer layer), which is divided further into sublayers. We assume an

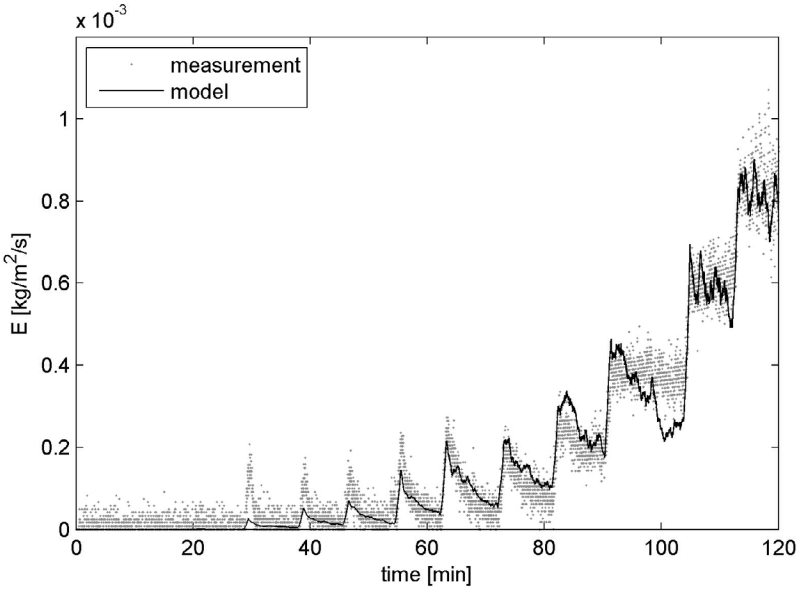

Figure 14. Comparison of stochastic erosion model with annular flume test C by *Jacobs* [2011]; the erosion rate varies with time, following 10-min steps in the bed shear stress [after *Van Prooijen and Winterwerp*, 2010].

initially normal distribution of the strength of the bed (critical shear strength of erosion), and we assume that strength and hydraulic stress distribution are mutually independent:

$$\mathrm{r}(\tau_{cr}) = \frac{1}{\sigma_{\tau,cr}\sqrt{2\pi}} \exp\left\{-\frac{\left(\tau_{cr} - \mu_{\tau,cr}\right)^2}{2\sigma^2_{\tau,cr}}\right\} \qquad (16)$$

in which $\mu_{\tau,cr}$ is the mean value of strength distribution and $\sigma_{\tau,cr}$ its standard deviation. Note that the left tail of the distribution is cut off as the critical bed shear stress cannot become negative. Basically, these strength parameters have to be obtained through calibration, or should follow from soil mechanical analyses, using bulk soil parameters – see below. The weaker fractions of the sediment bed erode when the bed shear stress exceeds a threshold, and armoring occurs, e.g., *Van Prooijen and Winterwerp* [2010]. We can extend this bed model and/or its interpretation by including a vertical gradient in parameters, accounting for the effects of consolidation, or a horizontal distribution, accounting for spatial inhomogeneties. Note that over time, the strength distribution of the bed changes, owing to erosion, consolidation, deposition, biological effects, etc.

6.2. Comparison With Annular Flume Data of *Jacobs* [2011]

[72] *Jacobs* [2011] carried out erosion experiments with mixtures of sand, silt and clay. In addition, all parameters required to determine the parameters of the erosion formulation (13) were established independently. Here we elaborate on sediment sample C, consisting of an artificial mixture of kaolinite clay (16%, D_{50} = 2 μm), silt (64%, D_{50} = 30 μm) and fine sand (20%, D_{50} = 180 μm). Hence, the median diameter of this mixture amounts to 55 μm. The erosion tests were carried out in an annular flume with a diameter of 3.7 m and a counterrotating bottom and lid. The flow velocity in the flume was increased from 0.01 till 1.14 m/s in time intervals of 10 min, and the experimental results are presented in Figure 14. It is important to realize that for instance in the seventh erosion interval (60–70 min), a sediment layer of 30 μm thickness only was eroded, if that erosion would have occurred evenly over the exposed sediment bed. During the last erosion interval (110–120 min) about 270 μm of material was eroded; in total, less than 1 mm was eroded, again, if evenly distributed over the entire annular flume. We will elaborate on this important observation in the next section.

[73] Jacobs' experiment C was simulated by *Van Prooijen and Winterwerp* [2010] with the model described in section 6.1, e.g., Figure 14. In that work, the model was calibrated varying the model parameters by trial and error, i.e., not linked to the soil mechanical properties of the sediment. In this section, a comparison is made between the calibrated values as obtained by *Van Prooijen and Winterwerp* [2010], and the values based on the formulations presented in the present paper (equations (9) and (13)).

[74] The erosion rate coefficient M_E (equation (13)) requires determination of the undrained shear strength c_u and the consolidation coefficient c_v, in addition to the dry density, the particle diameter and the sediment volume concentration. These parameters were determined by *Jacobs* [2011] as follows: $c_v = 8.0{\cdot}10^{-7}$ m^2/s; c_u = 0.2 kPa; ϕ_s = 0.5; ρ_{dry} = 1300 kg/m^3; and D_{50} = 55 μm. Note that in particular c_v shows large scatter ($1.0{\cdot}10^{-7}$ m^2/s < c_v < $8.0{\cdot}10^{-6}$ m^2/s), whereas the scatter for c_u is much smaller, estimated at 0.1 kPa < c_u < 0.3 kPa. From the mean values, an erosion depth δ_e of about 1 mm (e.g., equation (11)), and a mean erosion coefficient of M_E = 0.005 s/m is established. Note that M_E may vary between 0.0004 s/m and 0.09 s/m, respectively, for loose muds to more densely packed granular sediment beds [*Jacobs*, 2011], further to the above mentioned scatter in soil parameters. *Van Prooijen and Winterwerp*

[2010] found a value of M_E = 0.009 s/m from the trial and error calibration of their model. This value is not only well within the M_E range mentioned above, but given this range is very close to the mean value of M_E = 0.005 s/m found by *Jacobs* [2011].

[75] Within the model by *Van Prooijen and Winterwerp* [2010], an active layer was introduced, which thickness Δ determines the time scale of changes in sediment composition within the bed: the larger Δ, the slower the bed composition varies. The composition of the active layer governs the erosion rate, as finer, hence weaker fractions are washed out from this layer first: a kind of armoring takes place in the model. It is therefore to be expected that Δ should be of the order of the characteristic particle size. For cohesive sediments, this is the floc size D_{50}. *Van Prooijen and Winterwerp* [2010] found, from calibration of their model, a value of Δ = 50 μm, indeed very close to the measured D_{50} of 55 μm.

[76] Note that the thickness of the active layer Δ is not equal to the erodible depth δ_e, as explained in section 4.2.

[77] The calibrated active layer thickness Δ for simulating the experiments of *Amos et al.* [1992], [see *Van Prooijen and Winterwerp*, 2010], also turned out to be close to the median particle diameter ($\sim$30 μm). In his consolidation/erosion model, *Sanford* [2008] presumes a top layer with a mass of 0.05 kg/m^2, which yields Δ = 42 μm, assuming a dry density of 1200 kg/m^3.

[78] The mean critical bed shear stress for erosion (equation (9)) is estimated at τ_{cr} = 1.1 Pa, using the Atterberg limits given by *Jacobs* [2011]. In the model by *Van Prooijen and Winterwerp* [2010], a distribution of the bed shear stress is prescribed. Initially, i.e., at the start of the erosion experiment, a Gaussian distribution is used with $\mu_{\tau,cr}$ = 0.4 Pa and $\sigma_{\tau,cr}$ = 1.3 Pa. As the left tail of this Gaussian distribution has to be cut off for $\tau_{cr} < 0$, the mean value of this distribution becomes $\langle\tau_{cr}\rangle$ = 1.0 Pa. This is close to the τ_{cr} = 1.1 Pa, obtained with equation (9). At the end of the erosion test, the distribution changed to an almost full Gaussian distribution due to armoring, with a mean value of $\langle\tau_{cr}\rangle$ = 2.8 Pa. No measurements were carried out to determine the plasticity index after erosion, so no posterosion estimate of the critical shear stress could be made.

[79] Overall, we found close agreement between values obtained from the erosion formulations in section 5 and the values found from calibration of the model by *Van Prooijen and Winterwerp* [2010]. There is however uncertainty in the determination of some parameters, especially c_v. Calibration of the erosion model will therefore always remain necessary, although the range is reduced.

7. Discussion and Conclusion

[80] In this paper, we propose a conceptual framework for the erosion of cohesive sediment beds by shear flow, accounting for floc erosion, surface erosion and mass erosion, and the transitions from one mode to the other. We focus on cohesive beds with PI > 7%, with little sand. A classification scheme is derived as well, based on an analysis of the turbulent fluctuations of the eroding shear stresses, and an assumption on a Gaussian distribution of the sediment's strength within the bed. Mean values of the erosion rate in the surface erosion regime are obtained from soil mechanical theory, assuming swelling of the (over consolidated) bed to its critical state.

[81] The probability density function of the turbulent fluctuations was calibrated against the results of wind tunnel experiments. The parameters of the Gaussian bed strength distribution have to be found through calibration against experimental erosion data. The parameters for the soil mechanical erosion model can be measured readily from soil samples, or may follow from consolidation theory. The latter enables implementation of the proposed classification scheme, together with the feed back between hydrodynamics and soil response into numerical models, assessing transport and fate of cohesive sediments in the natural environment. In this approach we exclude the occurrence of fluid mud: at the solid bed, turbulence continues to be fully produced.

[82] We can summarize the transition between the various modes of erosion as follows: $0.5\tau_{cr} > \bar{\tau}_b$, stable bed; $0.5\tau_{cr} < \bar{\tau}_b < \tau_{cr}$, floc erosion; $\tau_{cr} < \bar{\tau}_b < 1.7\tau_{cr}$, floc and surface erosion; $\bar{\tau}_b > 1.7\tau_{cr}$, surface erosion; and $\sigma_{dyn} > \sim(2\text{–}5)c_u$, mass erosion (entrainment), where $\bar{\tau}_b$ is the mean bed shear stress induced by the turbulent water movement, and σ_{dyn} is the dynamic pressure. Note that this scheme is slightly different from the one presented by *Jacobs* [2011]. This schematization can also account for either depth-limited or unlimited erosion, as well as for stratified beds [e.g., *Sanford and Maa*, 2001]. At larger stresses (i.e., $\bar{\tau}_b > 1.7\tau_{cr}$), the model converges toward the linear erosion relation (2) (e.g., equation (13)). This linear erosion law is the result of a linear interpolation between drained and undrained strength (e.g., Figure 12); a nonlinear interpolation would yield a nonlinear erosion formula.

[83] *Van Prooijen and Winterwerp* [2010] also introduced a distribution function for the critical shear stress for erosion r(τ_{cr}). Its definition is straightforward for virgin beds. However, for beds subject to ongoing erosion and deposition, we have no tools (yet) available to quantify r(τ_{cr}). Therefore, we do not elaborate on this further. Moreover, if r(τ_{cr}) would be very wide, i.e., with large spatial variations in τ_{cr}, it will be difficult to define a characteristic distribution, as it will be difficult to measure typical values.

[84] The larger uncertainty in the erosion model follows from the scatter in the consolidation coefficient c_v, which may vary by orders of magnitude. This scatter is intrinsic to cohesive sediments. *Winterwerp and van Kesteren* [2004] present a graph relating normalized permeability ($k^* = k(1 + e)$), in which k = permeability and e = void ratio, with liquidity index LI. In particular for the softer sediments (larger LI), scatter in measured values of k^* is huge. This scatter is representative for the scatter in c_v, as k and c_v are closely related.

[85] The scatter in undrained shear strength c_u is smaller, though large gradients may build up within the bed during consolidation. Fortunately, such gradients are likely to be smoothed out by, e.g., bioturbation in the real world.

[86] During the erosion tests described in this paper, layers of a fraction of one millimeter are eroded, if we assume that the sediment is evenly (homogeneously) eroded. Such small numbers hold for the real world as well. This necessarily implies that spatial inhomogeneties must play an important role in the mean response of a sediment bed to shear flow.

[87] The observations in the two preceding paragraphs imply that the current framework for shear flow–induced erosion can give first-order estimates of erosion rates only. Therefore, when applied in, e.g., a (numerical) model, fine tuning of the parameters calibrating that model will remain a necessity.

[88] The functional relation of the erosion rate to easily measurable soil mechanical parameters provides a tool to establish gradients in erodibility at smaller or larger spatial scales.

[89] We note that in tidal environments, a soft, fluffy layer is formed on the bed around slack water, with thickness typical of a few mm, to one cm, at most. This fluffy layer is in equilibrium with the fine sediments suspended in the water column, being re-entrained during accelerating tide. The present scheme does not account for this re-entrainment, as this fluffy layer is too soft to obey the soil mechanical response described in this paper. However, the variations of this fluffy layer over longer time scales, e.g., spring-neap cycles, seasonal variations, can be addressed within the proposed framework.

[90] We note that *Partheniades* [2010] summarizes earlier work, carried out in the 1950s and 1960s on the erodibility of cohesive sediment beds, and efforts to relate critical shear stresses for erosion to the plasticity index, and erosion rates to bulk density, clay content and vane strength. Partheniades concluded that the macroscopic shear strength (vane strength) cannot be used as a proxi for the critical shear strength for erosion, as this macroscopic strength is 2 to 3 orders of magnitude larger than the critical shear strength. This observation is consistent with our conclusion that for not too soft soils the undrained shear strength is indeed much larger than the drained strength. Also, according to Partheniades, the Atterberg limits would not reflect the internal structure of a cohesive sediment bed, and are therefore not very useful either. However, the literature contains an overwhelming amount of data relating the soil mechanical parameters required in our method to the Atterberg limits. Partheniades therefore discarded correlations of erodibility parameters with soil mechanical properties, even though he claims that the results of many of the experiments discussed in his summary did suffer from experimental deficiencies. We believe we have argued, and shown that Partheniades was too pessimistic.

[91] Our framework requires determination of particle size distribution, in–situ bulk density, vane strength (remolded shear strength), consolidation coefficient and Atterberg limits. This framework therefore allows for collecting space-covering data on the erodibility of fairly large domains at relatively limited costs, as the bulk parameters are fairly inexpensive to be determined in the laboratory, following standardized procedure. These analyses can be carried out on bed grab samples (Van Veen grab): the samples may be stirred (remolded), as long as the in situ water content is not altered. These bulk parameters, moreover, account implicitly for the effects of organics within the bed, and some chemical effects as well. However, we must realize that the armoring effect of macrophytobenthos on intertidal areas cannot be captured easily with the proposed procedure, as microphytobenthos migrates from the bed surface into the bed, and back, depending on the stage of the tide. Yet, microphytobenthos may have a large effect on the stability of cohesive sediment beds, in particular on intertidal (mud) flats.

[92] Generally, muddy beds are fairly flat and hydraulically smooth. This implies that the effect of waves is then limited to the shear by the orbital motion. However, when the bed becomes irregular, dynamic pressures become important and erosion rates may grow rapidly.

[93] We appreciate that the volume of data sustaining the proposed erosion scheme is limited, in particular as we propose to describe the bed properties through a strength distribution. On the other hand, timely publication may stimulate other researchers to use our scheme, so that an extensive experimental data set for validation may be built up rapidly.

[94] The scheme presented here is valid for purely cohesive beds. *Jacobs* [2011] shows that the scheme may be extended to sand-mud mixtures at the transition between cohesive to a more granular behavior. In case of noncohesive beds, i.e., sand beds with small fractions of cohesives, another approach is required, such as proposed by *Van Kessel et al.* [2011]. In that model, a two-layer schematization is used accounting for seasonal effects through the buffering of fines in either layer. Such a two-layer schematization is also suitable to account for the dynamics of the fluffy layer described above.

Notation

A activity [−].
c true cohesion [Pa].
c_d drained shear strength [Pa].
c_u undrained shear strength [Pa].
c_v consolidation/swelling coefficient [m^2/s].
C_c compression index [−].
C_s swell index [−].
D_{50} median particle diameter [m].
E erosion rate [$kg/m^2/s$].
E_f floc erosion rate [$kg/m^2/s$].
e void ratio [−].
LI liquidity index [%].
LL liquid limit [%].
M erosion parameter [$kg/m^2/s$].
M_E erosion parameter [s/m].
n_f fractal dimension [−].
PI plasticity index [−].
PL plastic limit [−].
p^w pore water pressure [Pa].
t time [s].
U characteristic velocity [m/s].
V_e erosion velocity [m/s].
V_s swelling rate [m/s].
W water content [%].
z vertical coordinate [m].
α coefficient in equation (4) [−].
α_i coefficient in equation (14) [−].
β coefficient in equation (4) [−].
β coefficient in equation(8) [−].
γ_{cr} coefficient in equations (7) and (8) [−].
$\dot{\gamma}$ shear rate [1/s].
Δ thickness active layer [m].
δ_e erosion depth [m].
δ_s swelling depth [m].

$\mu_{t,cr}$ median critical shear stress for erosion [Pa].
ρ_b bulk density [kg/m^3].
ρ_{dry} dry bed density [kg/m^3].
ρ_w water density [kg/m^3].
σ normal stress [Pa].
σ_{dyn} dynamic stress [Pa].
σ_i normal principal stress [Pa].
$\sigma_{\tau,cr}$ standard deviation critical shear stress for erosion [Pa].
τ shear stress [Pa].
τ_B Bingham strength [Pa].
τ_b bed shear stress [Pa].
τ_{cr} critical shear stress for erosion [Pa].
τ_y yield strength [Pa].
ϕ angle of internal friction [deg].
ϕ_s solid's volume concentration [−].
ξ_0 critical clay content for cohesion [−].
ξ^{cl} clay content [−].
$\circ'$ parameter related to effective stresses.
$\bar{\circ}$ *t*urbulence-mean quantity.
$\langle \circ \rangle$ spatial mean quantity.

[95] **Acknowledgments.** Part of this work has been carried out within the framework of the project DCB6334 of the Dutch Technology Foundation STW. We wish to acknowledge the detailed and constructive comments and subsequent encouragements by Thomas Herbers (JGR Editor), Tom Hsu (Associate Editor), and the reviewers Larry Sanford and Chris Cherwood. The soil mechanical section in this second version of our manuscript has been reviewed in detail by M. Hicks.

References

Amos, C. L., G. R. Daborn, H. A. Christian, A. Atkinson, and A. Robertson (1992), In situ erosion measurements on fine-grained sediments from the Bay of Fundy, *Mar. Geol.*, *108*, 175–196, doi:10.1016/0025-3227(92)90171-D.

Ariathurai, C. R., and K. Arulanandan (1978), Erosion rates of cohesive soils, *J. Hydraul. Div. Am. Soc. Civ. Eng.*, *104*(2), 279–282.

Christensen, R. W., and B. M. Das, (1974), Hydraulic erosion of remoulded cohesive soils, in *Soil Erosion: Causes and Mechanisms, Preventions and Control*, *Spec. Rep. 135*, pp. 8–19, Natl. Res. Counc., Washington, D. C.

Croad, R. N. (1981), Physics of erosion of cohesive soils, *Rep. 247*, Dep. of Civ. Eng., Sch. of Eng., Univ. of Auckland, Auckland, New Zealand.

Fernandez Luque, R., and R. Van Beek (1976), Erosion and transport of bed-load transport, *J. Hydraul. Res.*, *14*(2), 127–144, doi:10.1080/00221687609499677.

Flemming, B. W. (2000), A revised textural classification of gravel-free muddy sediments on the basis of ternary diagrams, *Cont. Shelf Res.*, *20*, 1125–1137, doi:10.1016/S0278-4343(00)00015-7.

Harrison, A. J. M., and M. W. Owen (1971), Siltation of fine sediments in estuaries, paper presented at XIV Congress, Int. Assoc. for Hydro-Environ. Eng. and Res., Paris.

Hill, R. (1985), *The Mathematical Theory of Plasticity*, Clarendon, Oxford, U. K.

Hoffmans, G. J. C. M., and H. J. Verheij (1997), *Scour Manual*, Balkema, Rotterdam, Netherlands.

Jacobs, W. (2011), Sand-mud erosion from a soil mechanical perspective, PhD dissertation, Delft Univ. of Technol., Delft, Netherlands.

Jacobs, W., P. Le Hir, W. G. M. Van Kesteren, and P. Cann (2011), Erosion threshold of sand-mud mixtures, *Cont. Shelf Res.*, *31*, 14–25, doi:10.1016/j.csr.2010.05.012.

Kandiah, A. (1974), Fundamental aspects of surface erosion of cohesive soils, PhD dissertation, Univ. of Calif., Davis.

Kranenburg, C. (1994), *An entrainment model for fluid mud*, *Commun. Hydraul. Geotech. Eng.*, vol. 93-10, Fac. of Civ. Eng., Delft Univ. of Technol., Delft, Netherlands.

Kranenburg, C., and J. C. Winterwerp (1997), Erosion of fluid mud layers—I: Entrainment model, *J. Hydraul. Eng.*, *123*(6), 504–511.

Krone, R. B. (1962), Flume studies of the transport of sediment in estuarial shoaling processes, final report, Hydraul. Eng. Lab., Univ. of Calif., Berkeley.

Krone, R. B. (1993), Sedimentation revisited, in *Nearshore and Estuarine Cohesive Sediment Transport*, *Coastal Estuarine Stud.*, vol. 42, edited by A. J. Mehta, pp. 108–125, AGU, Washington, D. C., doi:10.1029/CE042p0108.

Kuijper, C., J. M. Cornelisse, and J. C. Winterwerp (1990), Erosion and deposition of natural muds–sediments from the Western Scheldt (Breskens), *Rep. 29*, Rijkswaterstaat Delft Hydraul. Cohesive Sed., Delft, Netherlands.

Kusuda, T., T. Umita, K. Koga, T. Futawatari, and Y. Awaya (1984), Erosional processes of cohesive sediment, *Water Sci. Eng.*, *117*, 891–901.

Lambe, T. W., and R. V. Whitman (1979), *Soil Mechanics, SI Version*, John Wiley, New York.

Le Hir, P., P. Cann, B. Waeles, H. Jestin and P. Bassoullet (2006), Instrumentation légère pour la mesure de l'érodabilité des sédiments vaseux ou sablo-vaseux [in French], paper presented at IXemes Journées Nationales Génie Côtier-Génie Civil, Cent. Fr. du Littoral, Brest, France.

Le Hir, P., Y. Monbet, and F. Orvain (2007), Sediment erodibility in sediment transport modeling: Can we account for biota effects?, *Cont. Shelf Res.*, *27*, 1116–1142, doi:10.1016/j.csr.2005.11.016.

Lick, W. (1982), The transport of contaminants in the Great Lakes, *Annu. Rev. Earth Planet. Sci.*, *10*, 327–353, doi:10.1146/annurev.ea.10.050182.001551.

Mazurek, K. A., N. Rajaratnam, and D. C. Sego (2003), Scour of a cohesive soil by submerged turbulent wall jets, *J. Hydraul. Res.*, *41*(2), 195–206, doi:10.1080/00221680309499961.

Mehta, A. J. (1981), Review of erosion function for cohesive sediment beds, paper presented at First Indian Conference on Ocean Engineering, Indian Inst. Technol. on Ocean Eng., Indian Inst. of Technol., Madras, India.

Mehta, A. J., and E. Partheniades (1975), An investigation of the deposition properties of flocculated fine sediment, *J. Hydraul. Res.*, *13*(4), 361–381, doi:10.1080/00221687509499694.

Mehta, A. J., and E. Partheniades (1979), Kaolinite resuspension properties, *J. Hydraul. Div.*, *104*(4), 409–416.

Merckelbach, L. M., and C. Kranenburg (2004), Equations for effective stress and permeability of soft mud-sand mixtures, *Geotechnique*, *54*(4), 235–243, doi:10.1680/geot.2004.54.4.235.

Mitchell, J. K. (1976), *Fundamentals of Soil Behavior*, John Wiley, New York.

Parchure, T. M., and A. J. Mehta (1985), Erosion of soft cohesive sediment deposits, *J. Hydraul. Eng.*, *111*(10), 1308–1326, doi:10.1061/(ASCE)0733-9429(1985)111:10(1308).

Partheniades, E. (1962), A study of erosion and deposition of cohesive soils in salt water, PhD dissertation, Univ. of Calif., Berkeley.

Partheniades, E. (1965), Erosion and deposition of cohesive soils, *J. Hydraul. Div. Am. Soc. Civ. Eng.*, *91*(1), 105–139.

Partheniades, E. (1986), A fundamental framework for cohesive sediment dynamics, in *Estuarine Cohesive Sediment Dynamics*, *Lecture Notes Coastal Estuarine Stud.*, vol. 14, edited by A. J. Mehta, pp. 219–250, Springer, Berlin.

Partheniades, E. (2010), *Cohesive Sediments in Open Channels: Properties, Transport, and Applications*, Elsevier, New York.

Sanford, L. P. (2008), Modeling a dynamically varying mixed sediment bed with erosion, deposition, bioturbation, consolidation, and armoring, *Comput. Geosci.*, *34*, 1263–1283, doi:10.1016/j.cageo.2008.02.011.

Sanford, L. P., and J. P.-Y. Maa (2001), A unified erosion formulation for fine sediments, *Mar. Geol.*, *179*, 9–23, doi:10.1016/S0025-3227(01)00201-8.

Sheng, P. Y. (1986), Modeling bottom boundary layer and cohesive sediment dynamics in estuarine and coastal waters, in *Estuarine Cohesive Sediment Dynamics, Lecture Notes Coastal Estuarine Stud.*, vol. 14, edited by A. J. Mehta, pp. 360–400, Springer, Berlin.

Smerdon, E. T., and R. P. Beasley (1959), The tractive force applied to stability of open channels in cohesive soils, *Res. Bull. 715*, Univ. of Mo., Columbia.

Sumer, B. M., and J. Fredsøe (2002), *The Mechanics of Scour in the Marine Environment*, *Adv. Ser. Ocean Eng.*, vol. 17, World Sci., River Edge, N. J.

Terzaghi, K. (1943), *Theoretical Soil Mechanics*, John Wiley, New York, doi:10.1002/9780470172766.

Torfs, H. (1995), Erosion of mud/sand mixtures, PhD dissertation, Katholieke Univ. Leuven, Leuven, Netherlands.

Van Kessel, T., J. C. Winterwerp, B. Van Prooijen, M. Van Ledden and W. Borst (2011), Modeling the seasonal dynamics of SPM with a simple algorithm for the buffering of fines in a sandy seabed, *Cont. Shelf Res.*, *31*(10), S124–S134.

Van Ledden, M. (2003), Sand-mud segregation in estuaries and tidal basins, PhD dissertation, Delft Univ. of Technol., Delft, Netherlands.

Van Ledden, M., W. G. M. van Kesteren, and J. C. Winterwerp (2004), A classification for erosion behavior of sand-mud mixtures, *Cont. Shelf Res.*, *24*, 1–11, doi:10.1016/j.csr.2003.09.002.

Van Prooijen, B. C., and J. C. Winterwerp (2010), A stochastic formulation for erosion of cohesive sediments, *J. Geophys. Res.*, *115*, C01005, doi:10.1029/2008JC005189.

van Rijn, L. C. (1984), Sediment pick-up functions, *J. Hydraul. Eng.*, *110*(10), 1494–1502, doi:10.1061/(ASCE)0733-9429(1984)110:10(1494).

Whitehouse, R., R. Soulsby, W. Roberts, and H. Mitchener (2000), *Dynamics of Estuarine Muds*, 210pp., Thomas Telford, London.

Whitlow, R. (2001), *Basic Soil Mechanics*, Harlow, Essex, U. K.

Winterwerp, J. C. (2007), On the deposition flux of cohesive sediment, in *Estuarine and Fine Sediment Dynamics; Proceedings of the 8th International Conference on Nearshore and Estuarine Cohesive Sediment Transport Processes*, *Proc. Mar. Sci.*, vol. 8, edited by J. Maa, L. Sanford, and D. Shoelhamer, pp. 209–226, Elsevier, New York.

Winterwerp, J. C., and W. G. M. van Kesteren (2004), *Introduction to the Physics of Cohesive Sediments in the Marine Environment*, *Dev. Sedimentol.*, vol. 56, Elsevier, New York.